Wireless passive high-temperature sensor based on multifunctional reflective patch antenna up to 1050 degrees centigrade

Haitao Cheng[a, *], Siamak Ebadi[b], Xinhua Ren[c] and Xun Gong[a, *]

[a] Antenna, RF and Microwave Integrated (AMRI) System Laboratory, Department of Electrical Engineering and Computer Science, University of Central Florida, Orlando, FL 32816, USA
[b] Intellectual Ventures, Bellevue, Washington 98005 U.S.A.
[c] Motorola Mobility Inc., Libertyville, IL 60048 U.S.A.

*Corresponding author. Tel.: +1 858 522 0178, E-mail: htcheng7@gmail.com (H. Cheng) and Tel.: +1 407 823 5762, E-mail: xun.gong@ucf.edu (X. Gong).

Abstract
A novel wireless passive temperature sensor based on a reflective patch is demonstrated up to 1050°C herein. This reflective patch acts as a patch resonator (temperature sensor) and an integrated antenna at the same time. The temperature sensing mechanism is the monotonic increase of the dielectric constant of alumina versus temperature, which reduces the resonant frequency of a patch resonator formed on such an alumina substrate. By properly designing the shape and dimensions of the patch, it can also act as a transmit/receive antenna for wireless passive sensing. Therefore, temperatures can be wirelessly sensed by measuring the resonant frequency of the temperature sensor using an interrogation antenna. This temperature sensor uses robust alumina and platinum materials for high-temperature applications. In addition, this wireless passive temperature sensor is simple in mechanical structure and low in profile, with the potential to be in conformal shape. A temperature sensor using this reflective patch was designed, fabricated and tested from 50 to 1050°C in ambient. The resonant frequency of the sensor decreases from 5.07 to 4.58 GHz, which corresponds to a dielectric constant change from 9.7 to 11.4 for the alumina substrate. The temperature measurement sensitivity is found to be 0.58 MHz/°C at 1050°C. Being wireless, passive, planar and low profile, the proposed high-temperature sensor can be used for various harsh-environment applications.

Keywords: harsh environment, microwave sensor, reflective patch antenna, wireless passive temperature sensor.

1. Introduction

Accurate online monitoring of temperatures as well as other physical parameters is highly desirable inside various harsh environments such as gas turbines [1], turbine engines [2] and nuclear reactors [3]. However, these harsh environments are typically characterized by high temperatures (>1000°C), corrosive gases (containing sodium, vanadium and sulfate), high pressures or nuclear radiation. Currently there are no commercially-available sensors which can survive these harsh environments and provide continuous monitoring. Novel sensor architectures and sensing mechanisms are necessary to achieve the aforementioned goal. Particularly, wireless sensors are highly desirable since they do not need failure-prone wire interconnections. In addition, they provide a lot of flexibility in mounting sensors at different locations.

Sensors based on active circuits can always provide longer wireless sensing distance. Recent advances in SiC [4] and GaN [5] have pushed the operating temperatures to 600°C. Nevertheless, in order to use these active-circuit-based sensors, complicated heat shielding and wire routing are required to house the active circuits below their critical operating temperatures [6]. Wireless passive sensors based on surface acoustic wave (SAW) materials are limited by the phase transformation and chemical stability of piezoelectric materials [7]. In [8], it was reported that SAW temperature sensors could sense temperatures up to 900°C. Alternatively, wireless passive sensors based on *LC* resonator and inductive coupling were used for high-temperature applications. Such sensors using low-temperature co-fired ceramics (LTCC) [9] and high-temperature co-fired ceramics (HTCC) [10] were reported to work up to 800°C and 600°C, respectively. It is noted that inductive coupling has many restrictions in terms of coil size, coil orientation and distance to metal surfaces, which limit their applications in harsh-environment applications.

The authors reported wireless passive sensing mechanisms using dielectrically-loaded resonators [11, 12]. When temperature rises, the dielectric constant of the material inside the sensor monotonically increases. As a result, by wirelessly detecting the resonant frequency, the temperature at the sensor can be extracted. However, the antennas were not integrated with sensors in [11, 12]. Using the resonator/antenna integration technique developed in [13-16], the authors demonstrated a wireless passive temperature sensor up to 1000°C by seamlessly integrating a slot antenna into a cavity resonator [17], which significantly reduced the sensor size. However, in [17], all six surfaces of the cavity resonator must be thoroughly metallized (except for the slot antenna) in order to guarantee the high quality (*Q*) factor of the cavity sensor, which is critical for wireless sensing distance and accuracy. This requirement on metallization may be a failure mechanism for the sensor in [17] if metals on the side faces or corners of the cavity resonator wear away during operations.

Different from the resonator/antenna in [17], a novel sensing mechanism is demonstrated in this paper by using a reflective

patch. This wireless passive temperature sensor has a simplified mechanical structure and relaxed metallization requirements using robust alumina substrate (melting temperature of 2072°C) and platinum (melting temperature of 1769°C). This reflective patch sensor is low profile, very simple in mechanical structure and easy to fabricate. In addition, the metallization area is just on the top and bottom sides of the sensor, which minimizes the chance of failure. This reflective patch sensor has its own ground plane, which allows the sensor to work even directly on metallic surfaces such as a blade inside a combustion turbine. Finally, conformal sensors using this reflective patch concept can also be developed for certain applications demanding curved shapes.

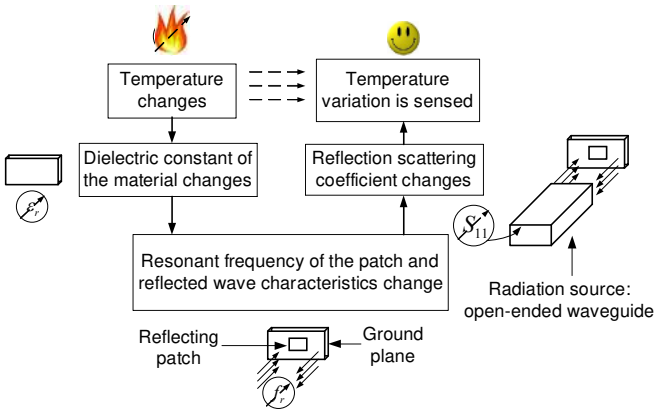

Fig. 1. Wireless sensing mechanism of the temperature sensor based on a reflective patch.

2. Principle of The Reflective Patch Sensor

As shown in Fig. 1, this new sensor is based on a reflective patch concept. Similar to the sensing mechanisms in [11, 12, 17], the resonant frequency of this sensor decreases versus temperature. An open-ended waveguide (OEWG) interrogation antenna sends out a wide-band signal to the temperature sensor. With proper designs, this patch resonator can work as an efficient radiator to receive the signal from the interrogator. The frequency components close to the resonant frequency of the patch, rather than being scattered right away, will enter the sensor, oscillate, and slowly decay over the time. These oscillating frequency components eventually leave the sensor through the patch radiator and are collected by the interrogation antenna. A time-domain (TD) gating technique will be used to isolate the signals corresponding to the resonant frequency of the sensor. In frequency domain, a maximum reflection from the sensor is expected after TD gating. A more detailed view of the sensor structure and interrogation antenna is shown in Fig. 2.

For a rectangular patch resonator operating in TM_{010} mode, its resonant frequency is approximately given by [18]:

$$f_r = \frac{c_0}{2L_{eff}\sqrt{\varepsilon_{eff}}} \tag{1}$$

in which L_{eff} is the effective patch length, ε_{eff} is effective relative permittivity of the patch substrate, and c_0 is the speed of light in vacuum. The patch and ground plane are made of platinum. To illustrate how the patch resonator works, its electric fields corresponding to the resonant frequency, a lower off-resonance frequency, and a higher off-resonance frequency, respectively, are plotted in Fig. 3, when this patch is interrogated by a *G*-band (WR-187, 3.95-5.85 GHz) OEWG antenna. It is apparent that at the resonant frequency of the patch, the RF energy enters the patch resonator and excites the electric field to the maximum intensity. In addition, the electric field reaches the maximum at the two shorter (radiating) edges of the patch. Accordingly, the equivalent magnetic current densities at these two edges are given by [18]:

$$M_s = -2\hat{n} \times E_a \tag{2}$$

These two magnetic dipoles radiate in the same way as a regular patch antenna except for the fact that there is no feeding port for the patch. The strong RF energy at the resonant frequency will be re-radiated from the patch and collected by the interrogation antenna.

In the next section, design details on the patch shape and dimensions in order to achieve the best sensing distance and resolution will be discussed.

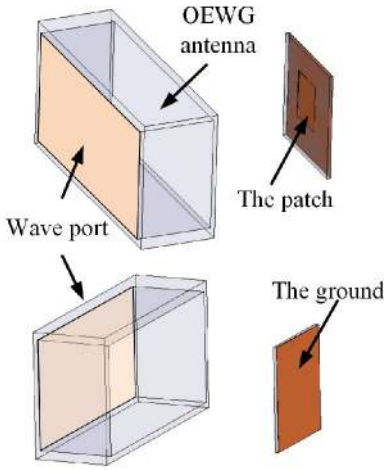

Fig. 2. 3-D views of the reflective patch sensor being interrogated by an OEWG antenna.

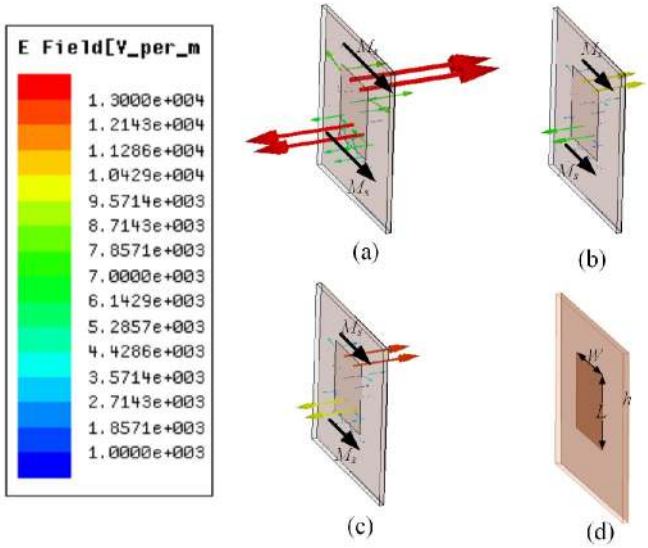

Fig. 3. Electric field distribution inside the dielectric substrate at (a) resonant frequency f_r = 5.05 GHz (b) lower off-resonance frequency f_1 = 5.00 GHz and (c) higher off-resonance frequency f_2 = 5.10 GHz. (d) Patch Dimensions. (L = 9.3 mm, W = 8 mm, h = 0.635 mm, and ε_r = 9.7)

3. Optimized Design of Thickness, Length and Width of the Patch Sensor

In this section, the effects from the patch length L, substrate thickness h and width W on the wireless passive reflective patch sensor will be studied.

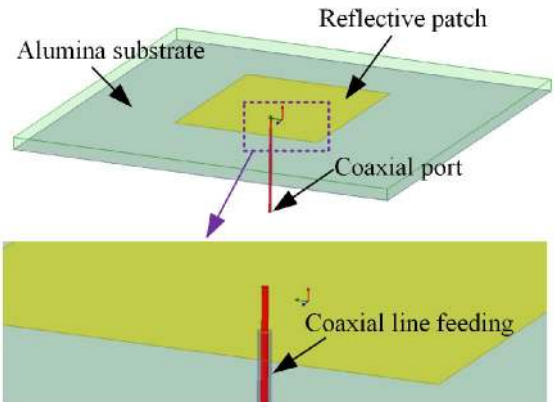

Fig. 4. A reflective patch coupled to a coaxial line to simulate the Q factor.

3.1. design of the patch length L

The patch length L can be calculated using [18]:

$$L = \frac{c_0}{2 f_r \sqrt{\varepsilon_{eff}}} - 2\Delta L \tag{3}$$

In which f_r is the resonant frequency of the patch; ε_{eff} is the effective dielectric constant; and ΔL is the difference between the physical length and effective length of the patch due to the fringing field effect. The analytical equations to calculate ε_{eff} and ΔL can be found in [18]. In this paper, f_r is designed to be 4.7 GHz at 1000°C. In the authors' earlier work [17], the dielectric constant of the alumina substrate was found to be 11.2 at 1000°C.

3.2. design of the substrate thickness h

The effect of h on the total Q factor (Q_T) of the reflective patch is investigated herein. Q_T is defined as the parallel combination of Q factors due to conductor loss (Q_c), dielectric loss (Q_d), radiation loss (Q_r) and surface wave loss (Q_{sur}). Q_T is a directly-measurable value from the interrogation antenna. Therefore, it is highly desirable to achieve higher Q_T which leads to better sensor resolution and longer wireless sensing distance. In order to simulate Q_T, a coaxial line is used to feed the patch in ANSYS High Frequency Structure Simulator (HFSS) simulations, as shown in Fig. 4. S_{11} at the coaxial port is illustrated in Fig. 5. Q_T can be extracted from S_{11} using the equation given by [19]:

$$Q_T = \frac{f_r}{f_2 - f_1}(1 + k) \tag{4}$$

in which, k is defined as:

$$k = \begin{cases} \dfrac{1 - 10^{-S_{11}^{\min}/20}}{1 + 10^{-S_{11}^{\min}/20}} & \text{undercoupled} \\ \dfrac{1 + 10^{-S_{11}^{\min}/20}}{1 - 10^{-S_{11}^{\min}/20}} & \text{overcoupled} \end{cases} \tag{5}$$

and the S_{11}^{ϕ} in Fig. 5 is given by:

$$S_{11}^{\phi} = 10 \log \frac{1 + 10^{-S_{11}^{\min}/10}}{2} \tag{6}$$

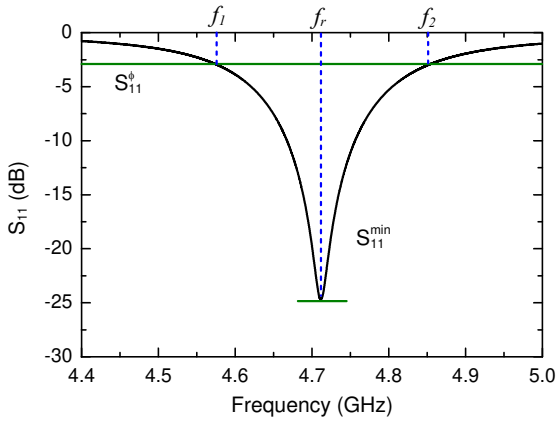

Fig. 5. Simulated S_{11} response of the coaxial port when the coaxial line is coupled to the patch. (L = W = 9.3 mm, h = 0.635 mm)

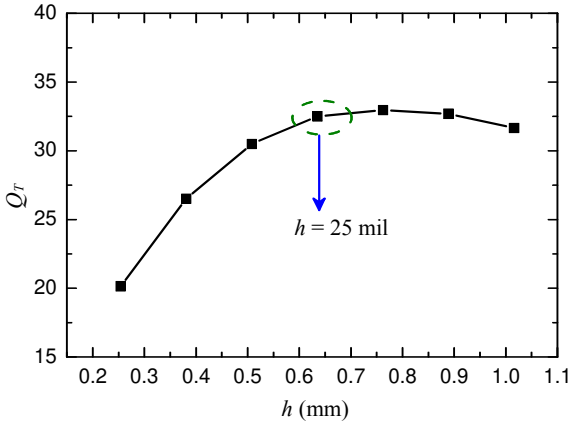

Fig. 6. Q_T versus alumina substrate thickness h. ($L = W = 9.3$ mm)

The relationship between Q_T and substrate thickness h for particular patch dimensions ($L = W = 9.3$ mm) is shown in Fig. 6. It is observed that Q_T increases versus h when $h < 0.75$ mm. Then Q_T starts to decrease when h further increases. This phenomenon can be explained using the following equations.

$$Q_c = h\sqrt{\pi f_r \mu_0 \sigma} \tag{7}$$

$$\frac{1}{Q_T} = \frac{1}{Q_r} + \frac{1}{Q_{sur}} + \frac{1}{Q_c} + \frac{1}{Q_d} \tag{8}$$

When h is small, the loss is dominated by the conductor loss. Typically radiation Q factor is higher for patch antennas on thinner substrates. In addition, there is not much surface wave excitation for thin substrates [20]. When the substrate becomes thicker, the conductor loss reduces. However, Q_r and Q_{sur} get smaller. It is noted that Q_d is approximately equal to $1/\tan\delta$ if the fringing field effect is neglected. Therefore, the maximum Q_T is expected at a certain optimum substrate thickness. We choose h = 0.635 mm (25 mil) since this is a commercially-available alumina substrate thickness and this h provides a near-maximum Q_T. In the simulations, the conductivity (σ) of the platinum paste is set to 5×10^5 S/m and the loss tangent ($\tan\delta$) of alumina substrate is defined as 0.012, which are extracted from the experiment results at 1000°C [17].

3.3. design of the patch width W

In this section, the effect of patch width W on Q_T and Q_{ext} of the patch is studied, in which Q_{ext} is defined as the parallel combination of Q_r and Q_{sur} and given by:

$$\frac{1}{Q_{ext}} = \frac{1}{Q_r} + \frac{1}{Q_{sur}} \tag{9}$$

As implied in Eq. (8), Q_{ext} is equal to Q_T when there are no metallic and dielectric losses. This can be realized by setting these two losses to be zero in HFSS simulations. Using the same method described in the Section 3.2, Q_{ext} can be extracted from simulated S_{11} at the coaxial port.

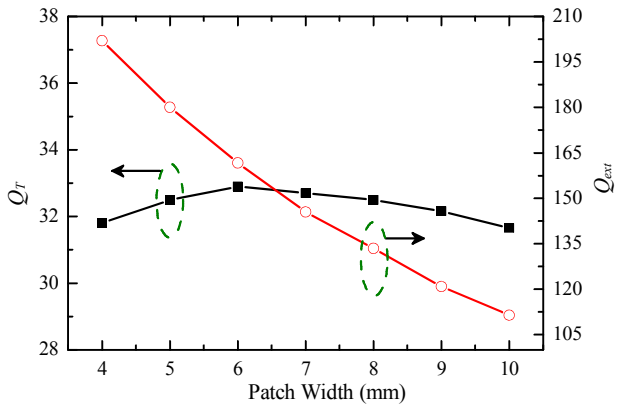

Fig. 7. Q_T and Q_{ext} versus patch width W. ($h = 0.635$ mm, $L = 9.3$ mm)

The relationship between W and Q_T/Q_{ext} is plotted in Fig. 7. The antenna efficiency is simply given as the ratio between these two Q factors and given by [18]:

$$\eta = \frac{Q_T}{Q_{ext}} \tag{10}$$

It is observed in Fig. 7 that Q_{ext} is generally much larger than Q_T, which implies that the metallic and dielectric losses are dominant. When W is small, the metallic loss is large due to the crowded current on the patch. Q_{ext} decreases with the patch width, implying higher antenna efficiency. Therefore, the maximum Q_T is expected at an optimum patch width, which is around 6 mm. However, the change in Q_T is very small for different W. By considering Eq. (10), a higher antenna efficiency requires a smaller Q_{ext}. Therefore, W = 8 mm is selected as the patch width to achieve near-maximum Q_T and higher antenna efficiency, while maintain TM_{010} still being the dominant mode for the patch (requiring $W < L$).

The final dimensions of the reflective patch sensor are L = 9.3 mm, W = 8 mm, and h = 0.635 mm.

4. Wireless Interrogation of the Reflective Patch Sensor

In this section, wireless interrogation of the reflective patch sensor is discussed. Fig. 8(a) shows simulated S_{11} responses for successive sensing distances between the OEWG antenna and reflective patch. The resonant frequency of the sensor is unidentifiable due to reflections from the OEWG antenna and scattering from the patch and ground. However, in the time domain as shown in Fig. 8(b), these interference signals can be separated from the sensor response due to a time delay between them. It is noted that Fig. 8(b) presents two S_{11} responses with and without the sensor in front of the OEWG, for a sensing distance of 30 mm. The main peak immediately after 0 ns is due to the reflection at the open aperture of the OEWG. For the case without the sensor, S_{11} quickly drops to the noise floor. When the reflective patch is present, it absorbs the incident wave from the OEWG first and then re-radiates back to the OEWG in a periodically-decaying manner. A TD gating window is set in between 1.3 and 20 ns. Similar gating procedures are carried out for sensing distances of 40, 50 and 60 mm, respectively. Finally, TD-gated signals are transformed back into the frequency domain and shown in Fig. 8(c). The resonant frequency of the sensor can be clearly identified and is independent of the sensing distance.

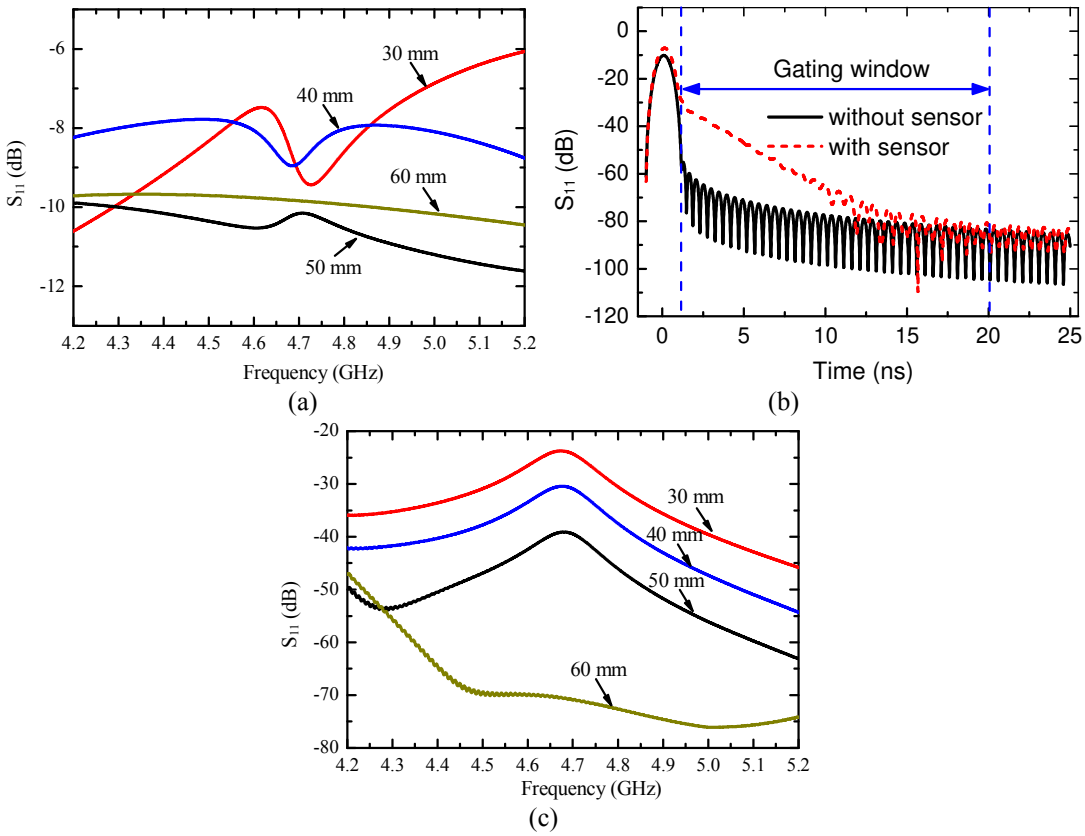

Fig. 8. (a) Simulated S_{11} at the input port of the OEWG before TD gating. (b) S_{11} responses of the OEWG in time domain with and without the sensor. (c) S_{11} responses of the OEWG for different sensing distances after the TD gating.

When patch dimensions and substrate thickness are fixed, the only parameter which can cause a resonant frequency change in the sensor is the dielectric constant of the alumina substrate. To illustrate this phenomenon, the dielectric constant of alumina is swept from 9.6 to 11.6 in HFSS simulations. The S_{11} of the OEWG corresponding to different dielectric constants shown in Fig. 9 clearly indicates a resonant frequency downshift. The sensor resonant frequency f_r versus dielectric constant is extracted from Fig. 9 and plotted in Fig. 10. The monotonic relationship between the dielectric constant and sensor resonant frequency is apparent, which provides the wireless temperature sensing mechanism.

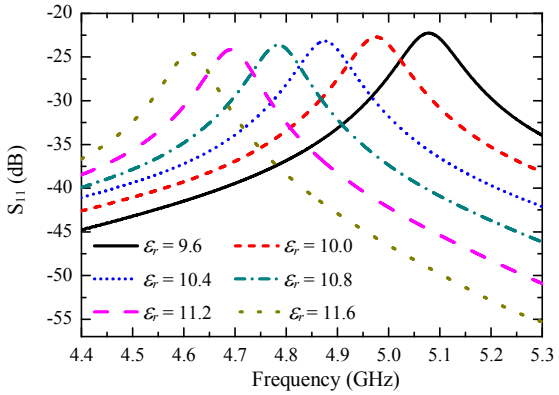

Fig. 9. Simulated S_{11} at the input port of the OEWG for various dielectric constants of the alumina substrate.

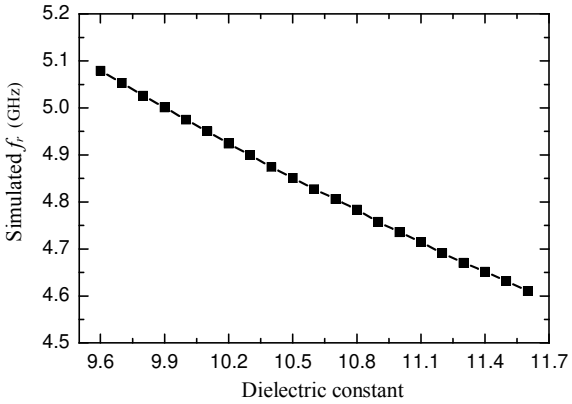

Fig. 10. Simulated resonant frequency of the patch sensor for various dielectric constants of the alumina substrate.

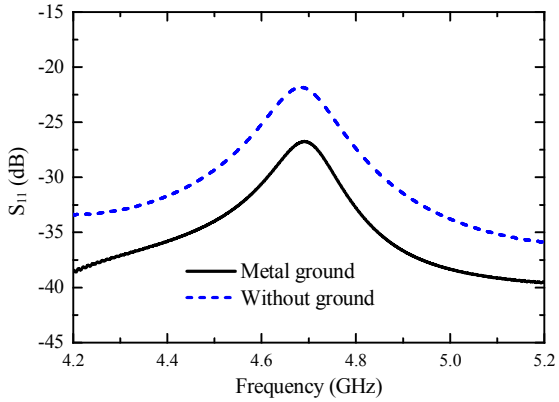

Fig. 11. Ground effect on the sensor response.

In many applications, sensors need to be mounted on highly-reflective surfaces such as engine blades or metallic walls. Therefore, it is highly desirable that the wireless passive temperature sensor studied herein can still work when it is mounted on the aforementioned surfaces. In HFSS simulations, for a sensing distance of 30 mm, a metallic ground plane of $\lambda_0 \times \lambda_0$ at 4.7 GHz

is placed behind the sensor. The comparison between the two cases with and without the ground plane is shown in Fig. 11. The resonant frequency of the sensor is barely influenced by the large ground plane. However, a 5-dB reduction in S_{11} is observed.

5. Fabrication and Measurement of the Wireless Reflective Patch Temperature Sensor

The patch sensor is fabricated on an alumina substrate (ADS-96R) with dimensions 21×21×0.635 mm^3 cut by an MTI Precision CNC Dicing/Cutting Saw (SYJ-400). A layer of platinum paste (ESL 5542) is applied and patterned on both top and bottom surfaces of the substrate to form the rectangular patch and ground plane, respectively. Then the alumina substrate with platinum paste is dried at 110ºC for 10 minutes and sintered at 980ºC for 10 minutes to form a dense platinum film. The ramp-up and ramp-down rates during the sintering are set to 10ºC/min. This procedure is repeated for six times to ensure continuous metal coverage and a total thickness of approximately 25 μm. The fabrication process is shown in Fig. 12 and described as follows. (a) The antenna layout is printed on a toner transfer paper by using a laser printer with 1200-dpi resolution. (b) The transfer paper is placed on an alumina substrate and then the ink is transferred to the alumina substrate using a thermal compression process. (c) Platinum paste is applied on the alumina substrate to form the antenna layout and ground plane. The sensor in the final form is shown in Fig. 12(d)-(e).

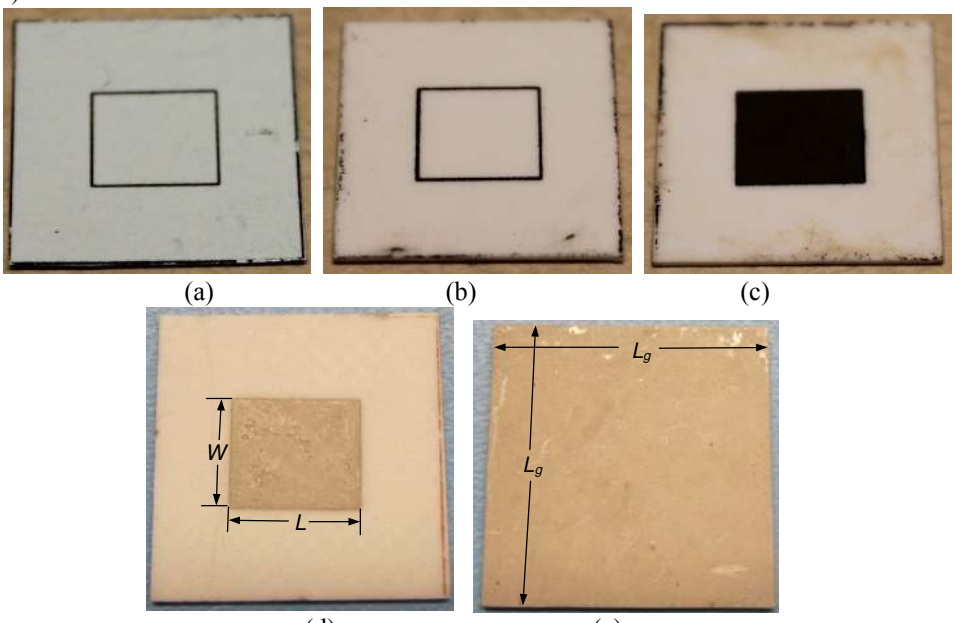

(a) (b) (c)

(d) (e)

Fig. 12. Fabrication process of the reflective patch sensor. (a) Antenna layout on transfer paper. (b) Antenna layout transferred to alumina substrate. (c) Patterned and dried platinum paste. (d) Top and (e) bottom view of the sintered reflective patch sensor. (W = 8 mm, L = 9.3 mm, L_g = 21 mm, and h = 0.635 mm).

The sensor testing is performed using a 2-inch-diameter heat pad (Micropyretics Heaters International Inc.), which can precisely control the temperature from 50 to 1050ºC. As shown in Fig. 13(a), the sensor is placed inside the heat pad and a *K*-type thermocouple (Omega HH11) is used to read the temperature and provide the feedback to the temperature controller. To prevent air convection and maintain a stable temperature environment, alumina boards are placed over the sensor to cover the heat pad as shown in Fig. 13(b).

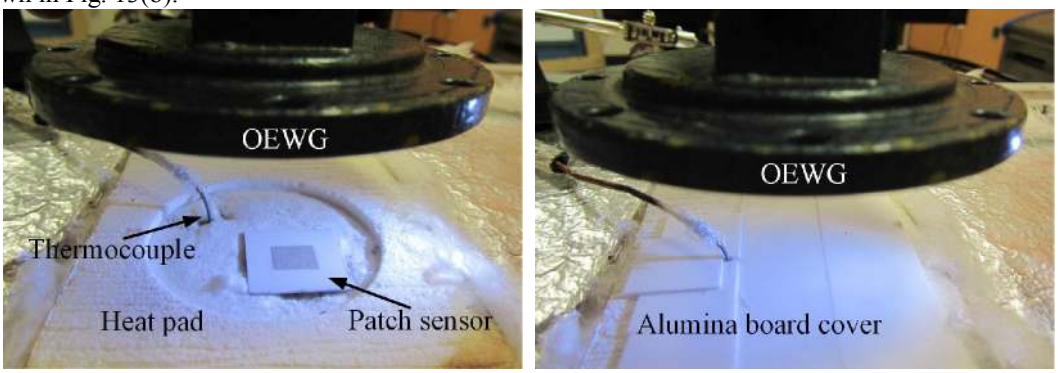

(a) (b)

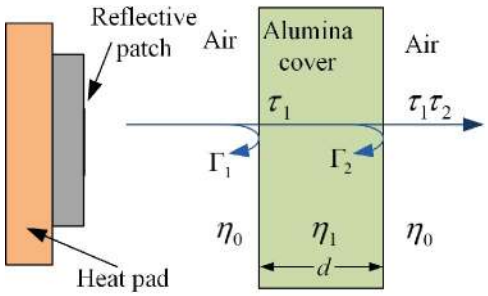

(c)

Fig. 13. Sensor measurement using an OEWG (a) without and (b) with alumina board cover. (c) Schematic showing the wave reflections due to the alumina board cover with a thickness d = 0.635 mm.

The re-radiated wave from the patch antenna experience a certain amount of reflections when passing through the alumina board cover as shown in Fig. 13(c). The total transmission coefficient can be calculated by:

$$|\tau_1\tau_2| = \left| \frac{(1+\Gamma_1)(1+\Gamma_2)}{e^{j\beta_2 d} + \Gamma_2 e^{-j\beta_2 d}} \right| \tag{11}$$

For the alumina board used in the measurements, this additional loss is found to be approximately 0.4 dB, which does not degrade the measurement results too much.

A one-port Short-Open-Load (SOL) calibration is performed with the reference plane at the input port of the *G*-band OEWG using an Agilent 40-GHz PNA-L (N5230A). The distance between the OEWG antenna and patch sensor is fixed at 30 mm for measurements at all temperatures from 50 to 1050°C. The S_{11} responses after TD gating for different temperatures are compared in Fig. 14. It is noted that the curve at 1000°C is higher than that of 800°C. This is due to the fact that the response at 1000°C is quite close to the noise floor therefore the S_{11} data for the 1000°C was taken at a slightly shorter sensing distance.

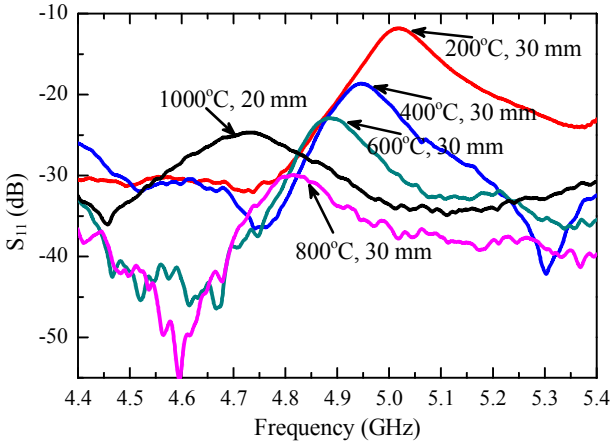

Fig. 14. Measured S_{11} at successive temperatures.

The resonant frequencies of the patch sensor versus temperature are plotted in Fig. 15. The measured resonant frequency monotonically decreases from 5.07 to 4.58 GHz, when the temperature is increased from 50 to 1050ºC, as shown in Fig. 15(a). The resonant frequency f_r is also simulated up to 1000°C, based on the dielectric constant of alumina characterized in [17]. The simulated and measured resonant frequencies closely match each other, with the largest deviation of 2% at 1000°C. The coefficient of thermal expansion (CTE) for alumina substrate is 8.2×10^{-6}/ºC, which corresponds to a 0.82% dimensional change of the substrate from 50 to 1050ºC. While the measured resonant frequency change in this temperature range is 9.7%. Therefore, the dielectric constant change is the dominant contributing factor to the resonant frequency variations. Additionally, the sensor sensitivity is extracted to be within the range of 0.41-0.58 MHz/°C as shown in Fig. 15(a). Q_T of the reflective patch sensor decreases from 64 to 30 for temperature from 50 to 1050°C as shown in Fig. 15(b). This is mainly due to the increased dielectric and metallic losses at higher temperatures. It is noted that each f_r or Q_T data is the average of ten independent measurements. The standard deviation of f_r in measurement is 5.9 MHz.

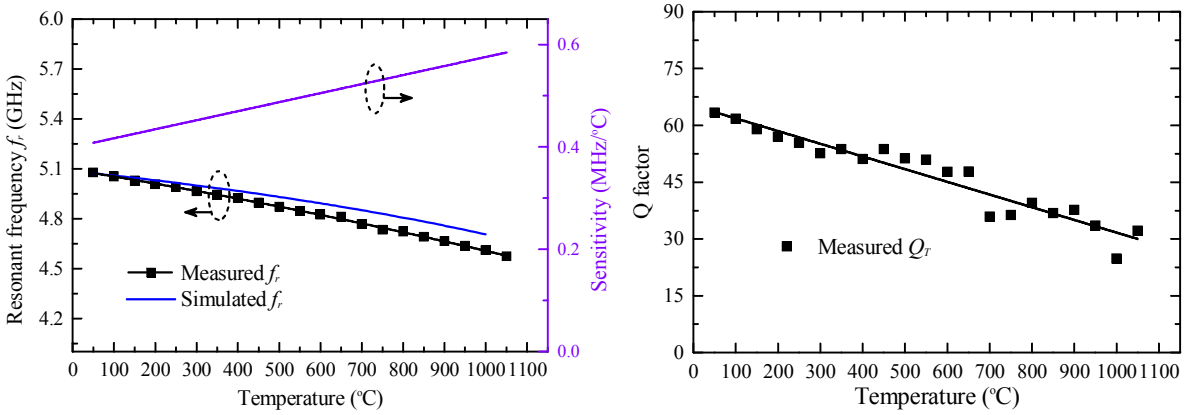

Fig. 15. (a) Measured and simulated resonant frequency of the sensor as well as measurement sensitivity, (b) measured Q_T versus temperature.

6. Conclusion

A novel wireless temperature sensor based on a reflective patch has been successfully designed, fabricated and measured up to 1050°C. This design represents the highest level of integration by using the reflective patch as both the temperature sensor and radiating antenna simultaneously. The simple mechanical structure, low profile, and stable materials will make this type of wireless passive sensors survive harsh environments. Temperature sensors using different robust materials can be realized using this reflective patch structure for specific applications. In addition, conformal temperature sensors on curved surfaces can also be formed using polymer-derived ceramics (PDC). In future works, we will study the stability and repeatability of this type of sensors mounted inside harsh environments.

Acknowledgement

The authors acknowledge the support from US Department of Energy under Grant DE-FE0001241.

References

[1] M. P. Boyce, *Gas Turbine Engineering Handbook, Third Edition*: Gulf Professional Publishing, 2006.

[2] R. E. Gorton, "Temperature measurement for aircraft-turbine-engine development," *Experimental Mechanics,* vol. 9, pp. 27N-34N, 1969.

[3] A. F. Fernandez, A. I. Gusarov, F. Berghmans, M. Decre, P. Me, A. Delchambre, M. Blondel, S. Bodart, and K. Lammens, "Temperature monitoring of nuclear reactor cores with multiplexed fiber Bragg grating sensors," *Opt. Eng.,* vol. 41, pp. 1246-1254, 2002.

[4] A. C. Patil, X.-a. Fu, M. Mehregany, and S. L. Garverick, "Fully-monolithic, 600 °C differential amplifiers in 6H-SiC JFET IC technology," in *IEEE CICC*, San Jose, CA, Sept. 13-16, 2009 pp. 73-76.

[5] P. Herfurth, D. Maier, L. Lugani, J.-F. Carlin, R. Rösch, Y. Men, N. Grandjean, and E. Kohn, "Ultrathin Body InAlN/GaN HEMTs for High-Temperature (600° C) Electronics," *IEEE Electron Device Lett.,* vol. 34, pp. 496-498, 2013.

[6] J. Yang, "A Silicon Carbide Wireless Temperature Sensing System for High Temperature Applications," *Sensors,* vol. 13, pp. 1884-1901, 2013.

[7] H. Fritze, "High-temperature piezoelectric crystals and devices," *J. Electroceramic.,* vol. 26, pp. 122-161, 2011.

[8] A. Canabal, P. Davulis, T. Pollard, and M. Pereira da Cunha, "Multi-sensor wireless interrogation of SAW resonators at high temperatures," in *IEEE Int. Ultrasonics Symp.*, San Diego, CA Oct. 11-14, 2010 pp. 265-268.

[9] E. D. Birdsell, J.-W. Park, and M. G. Allen, "Wireless ceramic sensors operating in high temperature environments," in *40 th AIAA/ASME/SAE/ASEE Joint Propulsion Conference*, Fort Lauderdale, FL, July 11-14, 2004

[10] Q. Tan, H. Kang, J. Xiong, L. Qin, W. Zhang, C. Li, L. Ding, X. Zhang, and M. Yang, "A Wireless Passive Pressure Microsensor Fabricated in HTCC MEMS Technology for Harsh Environments," *Sensors,* vol. 13, pp. 9896-9908, 2013.

[11] X. Ren, S. Ebadi, and X. Gong, "A single-antenna wireless passive temperature sensing mechanism using a dielectrically-loaded resonator," in *IEEE AP-S Int. Symp.*, Chicago, IL, July 8-14, 2012 pp. 1-2.

[12] X. Ren, S. Ebadi, H. Cheng, Y. Chen, L. An, and X. Gong, "Wireless resonant frequency detection of SiCN ceramic resonator for sensor applications," in *IEEE AP-S Int. Symp.*, Spokane, WA, July 3-8, 2011 pp. 1856-1859.

[13] H. Cheng, S. Ebadi, X. Ren, Y. Yusuf, and X. Gong, "A compact wireless passive sensing mechanism based on a seamlessly integrated resonator/antenna," in *IEEE AP-S Int. Symp.*, Spokane, WA, July 3-8, 2011 pp. 1350-1353.

[14] H. Cheng, Y. Yusuf, and X. Gong, "Vertically Integrated Three-Pole Filter/Antennas for Array Applications," *IEEE Antennas Wireless Propag. Lett.,* vol. 10, pp. 278-281, 2011.
[15] H. Cheng, S. Ebadi, and X. Gong, "A wireless pressure sensor design using a microwave cavity resonator," in *IEEE AP-S Int. Symp.*, Chicago, IL, July 8-14, 2012 pp. 1-2.
[16] Y. Yusuf, C. Haitao, and G. Xun, "Co-designed substrate-integrated waveguide filters with patch antennas," *IET Microwaves, Antennas & Propagation,* vol. 7, pp. 493-501, 2013.
[17] H. Cheng, S. Ebadi, and X. Gong, "A Low-Profile Wireless Passive Temperature Sensor Using Resonator/Antenna Integration Up to 1000°C," *IEEE Antennas Wireless Propag. Lett.,* vol. 11, pp. 369-372, 2012.
[18] C. A. Balanis, *Antenna theory: analysis and design*: John Wiley & Sons, 2012.
[19] R. J. Cameron, C. M. Kudsia, and R. R. Mansour, *Microwave filters for communication systems: fundamentals, design, and applications* vol. 1: Wiley-Interscience, 2007.
[20] R. Garg, P. Bhartia, I. Bahl, and A. Ittipiboon, *Microstrip antennas design handbook*: Artech House, 2001.

Haitao Cheng received the B.S. degree in electrical engineering from University of Electronic Science and Technology of China (UESTC), Chengdu, China, and M.S. degree in microelectronics from Shanghai Institute of Microsystem and Information Technology, Chinese Academy of Sciences, China (CAS), in 2006 and 2009, respectively. He received the Ph.D. degree in electrical engineering from University of Central Florida (UCF). His research interests include wireless passive sensors, high-Q resonators and filters, antennas, and phased arrays. He has served as a reviewer for several journals, including TMTT, AWPL, JMEMS, JMM, etc. He was the president of the Orlando student chapter of International Microelectronics and Packaging Society (IMAPS).

Siamak Ebadi received the B.S. degree from K. N. Toosi University of Technology (KNTU), Tehran, Iran, in 2003 and the M.S. and Ph.D. degrees from Tarbiat Modares University (TMU), Tehran, Iran, in 2005 and 2009, respectively, all in electrical engineering.

He is currently with the Metamaterials Commercialization Center (MCC) at Intellectual Ventures, Bellevue, WA, performing transformational research on new applications of Metamaterials in RF, Electromagnetics and Antennas. Prior to joining IV, he was with Antennas, RF and Microwave Integrated Systems (ARMI) laboratory at the department of Electrical Engineering and Computer Science (EECS), University of Central Florida (UCF) from 2010 to 2012 as a postdoctoral research associate where he conducted research on wireless high-temperature sensors and reconfigurable phased array and reflectarray antennas.

In 2008, he was involved in the European Commission's Agile Reflectarray Antennas for Security and Communications (ARASCOM) project designing reconfigurable reflectarray antennas as a researcher at University of Perugia, Italy.

His research interests include different fields of antenna design and electromagnetics including Metamaterials, phased array, slot array and reflectarray antennas as well as high-temperature wireless sensors.

Siamak Ebadi is a member of IEEE Antennas and Propagation (AP) and Microwave Theory and Technique (MTT) societies. He is currently the chair for AP/MTT/ED chapter in Seattle and held the chair position for AP/MTT chapter in Orlando, Florida from 2010 to 2012. He has been a reviewer for IEEE Antennas and Wireless Propagation Letters (AWPL), IEEE Transactions on Antennas & Propagation (TAP), IEEE Antennas and Propagation Society (AP-S) Magazine, IEEE Transaction on Microwave Theory and Techniques (TMTT), IEEE Wireless Communications Letters, and Elsevier International Journal of Electronics and Communications. He has been on the steering committee of IEEE Wireless and Microwave Technology Conference (Wamicon) 2012, IEEE APS/URSI 2013 conference and IEEE International Microwave Symposium (IMS) 2014.

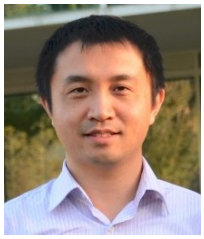

Xinhua Ren (S'06) received the B.S. degree in electrical engineering from the University of Science and Technology of China, Hefei, China, in 2006, and the Ph.D degree in electrical engineering from the University of Central Florida, Orlando, FL, in 2012. He was a graduate research assistant in the Antenna, RF & Microwave Integrated Systems Lab at the University of Central Florida, where he was involved with developing wireless passive micro-sensors for high-temperature applications. He is currently a Sr. Staff RF Engineer at Motorola Mobility, Chicago, IL. His research interests include electrically small antennas, wireless microwave sensors, and RF front-ends.

Xun Gong (S'02-M'05-SM'11) received the B.S. and M.S. degrees in electrical engineering from FuDan University, Shanghai, P.R. China, in 1997 and 2000, respectively, and the Ph.D. degree in electrical engineering from The University of Michigan at Ann Arbor in 2005.

He is currently an Associate Professor of Electrical Engineering and Computer Science (EECS) at University of Central Florida (UCF) and Director of the Antenna, RF and Microwave Integrated Systems (ARMI) Laboratory. He joined UCF as an assistant professor in 2005. He worked at Air Force Research Laboratory (AFRL) in Hanscom, MA in 2009 under the support of Air Force Office of Scientific Research (AFOSR) Summer Faculty Fellowship Program (SFFP). He was with the Birck Nanotechnology Center at Purdue University, West Lafayette, IN, as a Post-Doctoral Research Associate in 2005. His research interests include microwave passive components and filters, sensors, antennas and arrays, flexible electronics, and packaging.

Dr. Gong has served on the Editorial Boards of IEEE Transactions on Microwave Theory and Techniques (TMTT), IEEE Transactions on Antennas and Propagation (TAP), IEEE Microwave and Wireless Component Letters (MWCL), and IEEE Antennas and Wireless Propagation Letters (AWPL). He is the associate editor of IEEE MWCL. He was the technical program committee (TPC) chair in the 2013 IEEE AP-S/URSI International Symposium and Operations chair in the 2014 IEEE MTT-S International Microwave Symposium (IMS). He was the general chair in the 2012 IEEE WAMICON. He was the IEEE AP/MTT Orlando Chapter Chair in 2007-2010. He has been the recipient of the NSF Faculty Early CAREER Award in 2009. He received the Research Incentive Award (RIA) at UCF in 2011. He was the recipient of the Teaching Incentive Program (TIP) Award at UCF in 2010. He received Outstanding Engineer Awards from IEEE Florida Council and Orlando Section, respectively, in 2009.